

# Evolution of the Magnetic Field Structure of the Crab Pulsar

Andrew Lyne,<sup>1\*</sup> Francis Graham-Smith,<sup>1</sup> Patrick Weltevrede,<sup>1</sup>  
Christine Jordan,<sup>1</sup> Ben Stappers,<sup>1</sup> Cees Bassa,<sup>1</sup> Michael Kramer<sup>1,2</sup>

<sup>1</sup> Jodrell Bank Centre for Astrophysics, School of Physics and Astronomy,  
University of Manchester, Manchester, M13 9PL, UK

<sup>2</sup> MPI für Radioastronomie, Auf dem Hügel 69, 53121 Bonn, Germany

\*To whom correspondence should be addressed; E-mail: andrew.lyne@manchester.ac.uk.

**Pulsars are highly-magnetised rotating neutron stars and are well-known for the stability of their signature pulse shapes, allowing high-precision studies of their rotation. However, during the past 22 years, the radio pulse profile of the Crab pulsar has shown a steady increase in the separation of the main pulse and interpulse components at  $0.62^\circ \pm 0.03^\circ$  per century. There are also secular changes in the relative strengths of several components of the profile. The changing component separation indicates that the axis of the dipolar magnetic field, embedded in the neutron star, is moving towards the stellar equator. This evolution of the magnetic field could explain why the pulsar does not spin down as expected from simple braking by a rotating dipolar magnetic field.**

The Crab pulsar (1) originated in the collapse of the core of a massive star in AD 1054, an event that was visible on Earth through the subsequent supernova explosion. Presently rotating at 30 times a second (2), intense beams of electromagnetic radiation from the magnetic poles of the neutron star sweep across the Earth (3), resulting in pulsed emission which has been

observed since 1969 at radio wavelengths and subsequently at optical, X-ray and gamma-ray wavelengths. The pulse profile is related to the shape of the beams which are determined by the magnetic field structure of the underlying star as it rotates (3). We have therefore sought changes in the radio pulse profile in order to investigate any evolution in the structure of the stellar magnetic field.

High-quality daily observations of the Crab pulsar (PSR B0531+21, J0534+2200) have been made since 1991 with the 13-m radio telescope at Jodrell Bank Observatory at a frequency of 610 MHz. These measurements are supplemented by less-frequent observations using the 76-m Lovell Telescope at the higher frequency of 1400 MHz, designed to monitor dispersion measure. These data comprise part of a consistent set of pulse timing observations at Jodrell Bank (4, 5) that have provided a complete record of the rotation of the pulsar since 1984, and are available as an ephemeris to other observers (6). The radio pulse profile (Fig. 1) consists of a pair of components, the main pulse (MP, at  $0^\circ$ ) and the interpulse (IP, at  $145^\circ$ ), which are closely associated with the components of the profiles observed in the high-energy regimes from optical to TeV gamma-rays (7). At the comparatively low radio frequency of 610 MHz there is also a steep-spectrum third component known as the precursor (PC, at  $-18^\circ$ ). This component is not detectable at 1400 MHz, although another, previously-identified component, the “low-frequency component” (LFC, at  $-37^\circ$ ) (8), is seen at both frequencies. The components HFC1 (at  $200^\circ$ ) and HFC2 (at  $260^\circ$ ) reported before (8) also appear in the 1400-MHz profile, but are too weak to be addressed in this study.

The temporal evolution of the separation between the MP and other components (9) can be seen in Fig. 2 (IP) and Fig. 3 (LFC and PC), while variations in the relative integrated flux densities of the pulse components are shown in Fig. 4. Secular changes are observed in all three diagrams. The component separations and relative flux densities, together with their rates of change measured over the 22 years, are presented in Table 1. In summary, the most notable

Table 1: The rotational positions and integrated flux densities of the interpulse (IP), precursor (PC) and low-frequency component (LFC) of the radio profile of the Crab pulsar. Values are given in columns 2 and 4 relative to the MP at epoch MJD=53,000 at 610 MHz and 1400 MHz. Columns 3 and 5 contain the rates of change of these two quantities respectively. Standard ( $1\sigma$ ) errors are given in parentheses after the values and are in units of the least significant quoted digit.

	Position ( $^{\circ}$ )	Rate of Change ( $^{\circ}/\text{century}$ )	Flux Ratio	Rate of Change ( $/\text{century}$ )
IP (610 MHz)	145.588(2)	+0.62(3)	0.5648(6)	-0.172(8)
IP (1400 MHz)	145.324(9)	+0.5(2)	0.265(1)	-0.17(3)
PC (610 MHz)	-18.415(17)	-0.6(3)	0.1967(6)	-0.226(11)
LFC (1400 MHz)	-37.43(7)	+11(2)	0.059(1)	-0.005(33)

features are that:

(i) the separation of the IP from the MP at 610 MHz has increased by  $0.14^{\circ}$ , corresponding to  $13 \pm 1 \mu\text{s}$  (Fig. 2), together with a consistent change at 1400 MHz.

(ii) the separation of the LFC from the MP at 1400 MHz has increased by  $2.4^{\circ}$ , corresponding to  $220 \pm 40 \mu\text{s}$  (Fig. 3A).

(iii) the flux density of the IP has decreased relative to that of the MP by  $\sim 6\%$  at 610 MHz and by  $\sim 13\%$  at 1400 MHz (Fig. 4A and Fig. 4B).

(iv) the flux density of the PC at 610 MHz has decreased relative to that of the MP by  $\sim 13\%$  (Fig. 4C).

The origins of the pulse components are within a co-rotating magnetosphere which is embedded in the neutron star and extends almost to the light cylinder, the cylindrical surface at which the co-rotation velocity would reach the velocity of light. The source of the PC is believed to be located over a magnetic pole, at a small fraction of the distance to the light cylinder. The MP and IP components of the high-energy (optical, X-ray and gamma-ray) profile originate

in two high-altitude gaps in the magnetosphere, at the boundary between magnetic field lines which close within the light cylinder and the open field lines which are closer to the magnetic poles. This emission occurs in an extended region along each gap, while the combined effect of propagation time along the gap and relativistic effects concentrates the observed source in to a caustic (10). While this broadly describes the emission, the exact distribution depends on the specific emission model (e.g. (11, 12, 13, 14, 15)). In the following, we construct a geometrical interpretation for the secular increase in the separation of the MP and IP radio emission. This is possible because the radio components are closely associated with the high energy emission, thereby suggesting that high energy models can be used to interpret the observed evolution of this separation.

The observed high-energy profile is a cut across a hollow conical surface of emission over one or both magnetic poles. The shape of the cone is determined by the inclination  $\alpha$  of the magnetic axis to the rotation axis, and the position of the cut depends on the viewing angle  $\zeta$ , which is measured from the rotation axis. There is good evidence from the geometry of the X-ray torus in the pulsar wind nebula seen around the pulsar (16) that the viewing angle  $\zeta$  is close to  $63^\circ$ . The observed secular increase of the separation between the IP and MP might be due to a change in viewing geometry due to precession (17) (on a timescale much larger than the 2.3% of the 960-year lifetime of the pulsar that our observations cover), or in  $\alpha$  (i.e alignment or counter alignment of the magnetic and rotation axes) or in the location within the magnetosphere of the source of emission. While a long-period free precession of the neutron star might provide an appropriate change in the beam geometry, not only are there theoretical arguments why it should not occur (18, 19), but no pulsar has been shown to display the phenomenon (e.g. (20)). Here we demonstrate that a change in  $\alpha$  will result in a self-consistent interpretation.

The shape of the beam of the Crab pulsar has been modelled by several authors (e.g. (14, 21, 22, 23)), resulting in a range of estimates of  $\alpha$  between  $45^\circ$  and  $70^\circ$ . Nevertheless, a common

feature of these models is a prediction that an increasing  $\alpha$  will result in an increasing peak separation (e.g. Figs. 5 and 2 in (22), from which it can be deduced that the peak separation is expected to change at a rate of about one degree per degree change in  $\alpha$ ), although the exact relationship is somewhat model-dependent. The observed secular increase of the separation therefore indicates that the dipole axis is moving towards orthogonality. The observed component separation is increasing from  $145.5^\circ$  towards the symmetrical value of  $180^\circ$  at a rate of  $0.62^\circ$  per century (Fig. 2). We therefore interpret our observation as an increase of  $\alpha$  at a comparable rate, at which rate the total change would have been about  $6^\circ$  during the lifetime of the pulsar so far.

It is difficult to relate the rapid apparent motion of the LFC, whose origin is not understood, to this geometric evolution in any detail. The changes in relative flux densities of the components are easier to understand because all the sources are highly coherent and are probably narrow beamed (24), so that small structural magnetospheric changes might cause large effects on the component flux densities.

The dipole magnetic field is embedded in the superconducting interior of the neutron star, either in the inner crust or in the core, and only a slow evolution can be expected. An evolution towards alignment rather than orthogonality is expected for a simple magnetic dipole. However, it has been pointed out that an evolution towards orthogonality may be expected because of the torque developed by the return current in the neutron star surface (e.g. (25)). We also note that the increasing slowdown torque due to increasing  $\alpha$  could at least in part explain the observed braking index value of 2.50 (5), rather than 3.0 expected for classic magnetic dipole braking (26), or may be related to the occurrence of glitches seen in the pulsar (27, 28). If the sole departure from such classic slowdown, in which the rate of change of rotation rate  $\dot{\nu} \propto \nu^3 \sin^2(\alpha)$ , is a secular change in  $\alpha$  at a rate  $\dot{\alpha}$ , the observed braking index  $n$  is given by  $n = 3 + 2\nu/\dot{\nu} \times \dot{\alpha}/\tan(\alpha)$ . Within the limitations of our model, the observed braking index can

be explained if  $\alpha$  increases at  $0.6^\circ$  per century, which is remarkably close to the rate of change in  $\alpha$  required to explain the secular change in the pulse separation.

These observations provide evidence for a progressive change in the magnetic inclination of an isolated pulsar. The precise measurement of the small change in pulse profile, which leads to this conclusion, has depended on a long and consistent series of observations of one of the youngest pulsars. It is unlikely that comparable measurements can be made on any other pulsar in the near future.

## References and Notes

1. D. H. Staelin, E. C. Reifenstein, III, *Science* **162**, 1481 (1968).
2. J. M. Comella, H. D. Craft, R. V. E. Lovelace, J. M. Sutton, G. L. Tyler, *Nature* **221**, 453 (1969).
3. T. Gold, *Nature* **218**, 731 (1968).
4. A. G. Lyne, R. S. Pritchard, F. G. Smith, *MNRAS* **233**, 667 (1988).
5. A. G. Lyne, R. S. Pritchard, F. G. Smith, *MNRAS* **265**, 1003 (1993).
6. A. G. Lyne, C. A. Jordan, M. E. Roberts, *The Jodrell Bank Crab Pulsar Ephemeris* (University of Manchester, Manchester, 2013). (<http://www.jb.man.ac.uk/pulsar/crab.html>).
7. A. A. Abdo, *et al.*, *ApJ* **708**, 1254 (2010).
8. Moffett, D. A. and Hankins, T. H., *ApJ* **468**, 779 (1996).
9. Materials and methods are available as supplementary material on Science Online.
10. M. Morini, *MNRAS* **202**, 495 (1983).

11. K. S. Cheng, C. Ho, M. Ruderman, *ApJ* **300**, 500 (1986).
12. R. W. Romani, I.-A. Yadigaroglu, *ApJ* **438**, 314 (1995).
13. A. G. Muslimov, A. K. Harding, *ApJ* **606**, 1143 (2004).
14. J. Dyks, B. Rudak, *ApJ* **598**, 1201 (2003).
15. R. W. Romani, K. P. Watters, *ApJ* **714**, 810 (2010).
16. C.-Y. Ng, R. W. Romani, *ApJ* **673**, 411 (2008).
17. D. I. Jones, N. Anderson, *MNRAS* **324**, 811 (2001).
18. J. Shaham, *ApJ* **214**, 251 (1977).
19. A. Sedrakian, I. Wasserman, J. M. Cordes, *ApJ* **524**, 341 (1999).
20. A. Lyne, G. Hobbs, M. Kramer, I. Stairs, B. Stappers, *Science* **329**, 408 (2010).
21. A. K. Harding, J. V. Stern, J. Dyks, M. Frackowiak, *ApJ* **680**, 1378 (2008).
22. K. P. Watters, R. W. Romani, P. Weltevrede, S. Johnston, *ApJ* **695**, 1289 (2009).
23. Y. J. Du, G. J. Qiao, W. Wang, *ApJ* **748**, 84 (2012).
24. A. G. Lyne, F. Graham-Smith, *Pulsar Astronomy, 4th ed.* (Cambridge University Press, Cambridge, 2012). P265.
25. V. S. Beskin, E. E. Nokhrina, *Ap&SS* **308**, 569 (2007).
26. W. W. Macy, Jr., *ApJ* **190**, 153 (1974).
27. B. Link, R. I. Epstein, *ApJ* **478**, L91 (1997).

28. M. P. Allen, J. E. Horvath, *ApJ* **488**, 409 (1997).
29. A. G. Lyne, R. S. Pritchard, F. Graham-Smith, *MNRAS* **321**, 67 (2001).
30. B. Kuzmin, B. Y. Lovosky, C. A. Jordan, F. G. Smith, *A&A* **483**, 13 (2008).

Pulsar research at JBCA is supported by a Consolidated Grant from the UK Science and Technology Facilities Council.

### **Supplementary Materials**

[www.sciencemag.org](http://www.sciencemag.org)

Materials and Methods

References (20,29,30)



## Materials and methods

The method of determination of the pulse shape parameters from the observed pulse profiles used here was similar to that described earlier (20). Each of the two pulse profiles shown in Fig. 1 was inspected and fitted with up to five Gaussian components, as required to provide satisfactory descriptions of the profiles. Two Gaussian components were used to describe each of the MP and IP and a single one for either the PC (at 610 MHz) or LFC (at 1400 MHz). Components which initially had these amplitudes, widths and relative positions were then fitted to each observed profile, by adjusting the values of the parameters in a least-squares minimisation process to produce a synthetic profile. From this synthetic profile, values of parameters such as component integrated flux densities and separations were determined and presented in Table 1 and Figs. 2-4. Note that this procedure has the virtue of applying a quasi-optimum filter to the data in order to minimise the effects of high-frequency noise in the profiles on the values of the parameters.

The radio pulse profile of the Crab pulsar at around 610 MHz suffers from a variable amount of multipath scattering from plasma in the Crab Nebula (29,30), causing significant asymmetric distortion of the profile. To first order this has no effect upon the measured component separations, since all components are delayed by the same amount. However, because of subtle differences in the underlying component structures, trials showed that increasing the amount of smoothing due to scattering resulted in small systematic changes in the measured separation of the MP and IP, amounting to  $(W_{50}-6.0)\times 0.035^\circ$ , where  $W_{50}$  is the FWHM of the MP in degrees. This correction was applied to the measured values of MP and IP separation. In about 5% of the observations, strong scattering caused  $W_{50}$  to increase to greater than  $7^\circ$ , in which cases the component positions were more poorly defined and the observations were discarded. For the remaining data, the average magnitude of the applied correction was  $0.008^\circ$ , notably smaller than the secular variations reported in this paper.

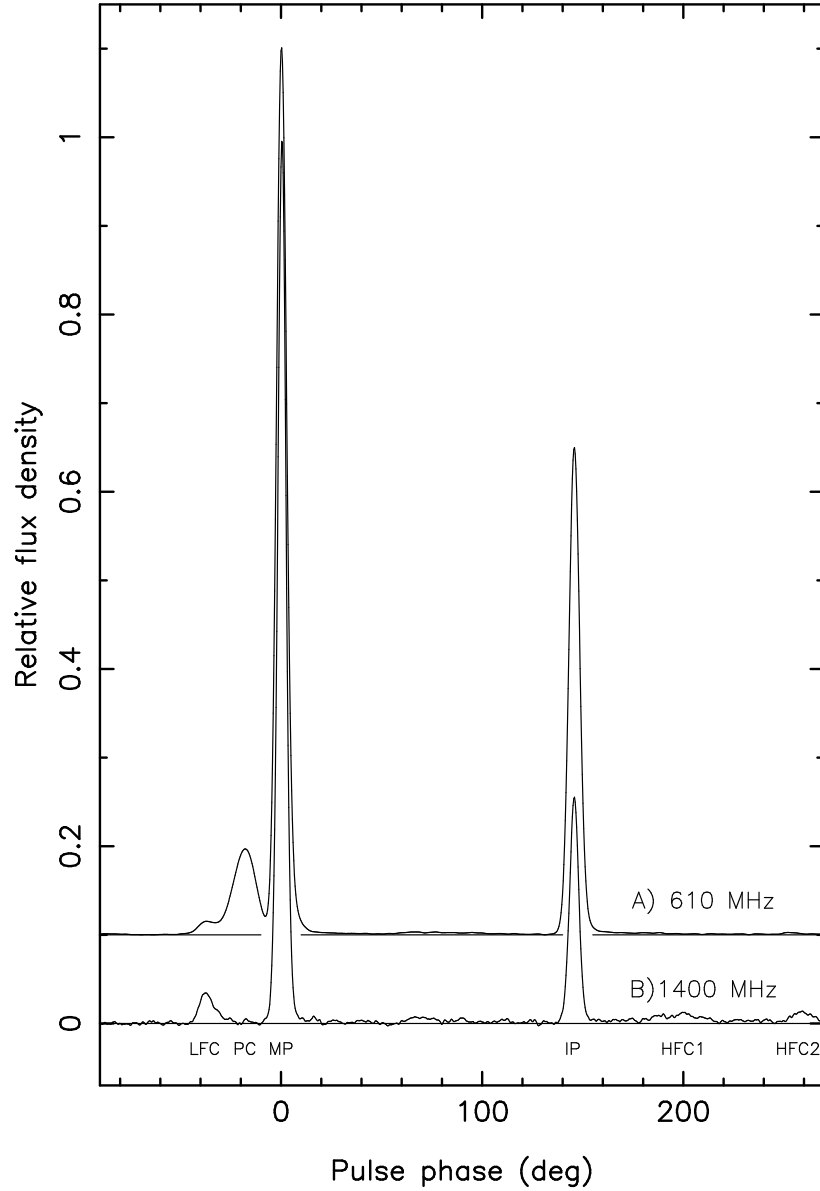


Figure 1: The average pulse profiles of the Crab pulsar. A) 610 MHz and B) 1400 MHz. The locations of the features discussed in the text are indicated below the profiles: the main pulse (MP) and interpulse (IP) lie at rotational phases  $0^\circ$  and  $145^\circ$ , while the precursor (PC) and Low-Frequency Component (LFC) lie at  $-18^\circ$  and  $-37^\circ$ , respectively.

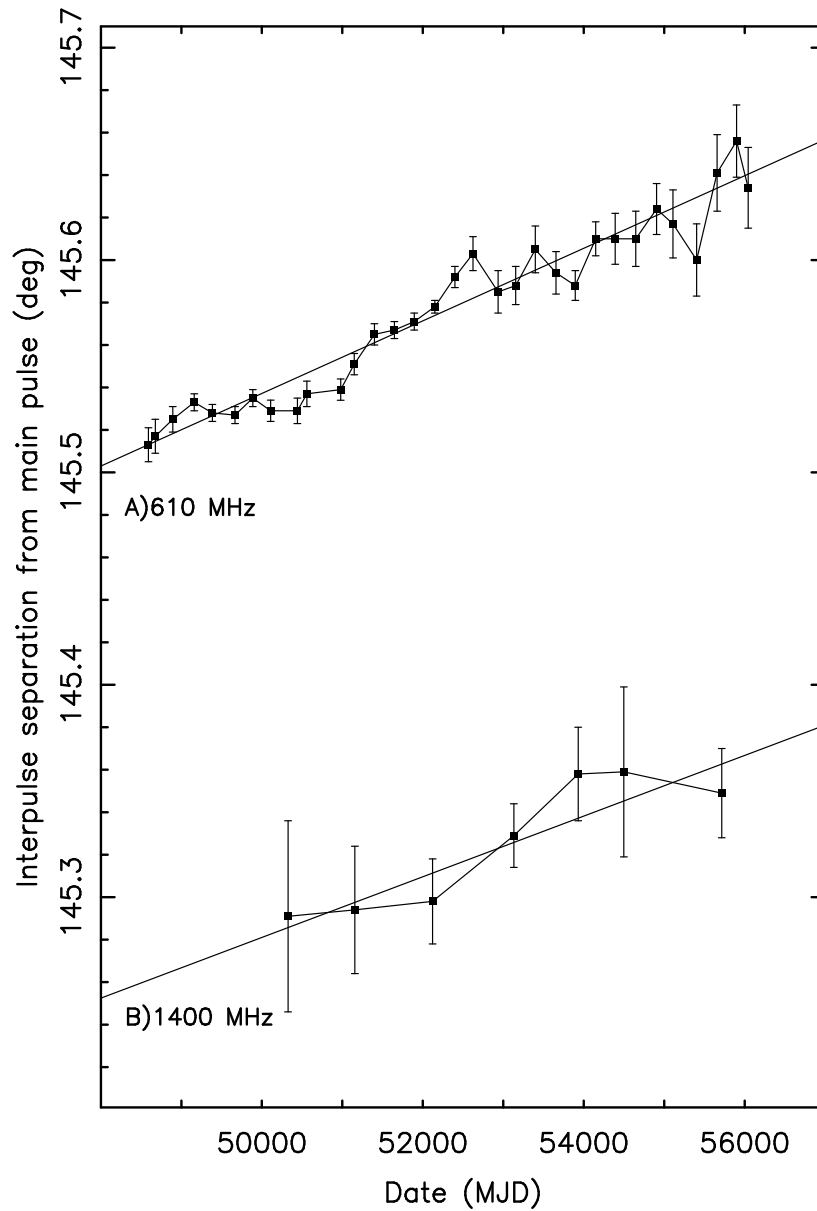


Figure 2: The rotational separation of the IP from the MP. A) 610 MHz and B) 1400 MHz. Data at 610 MHz are displayed as mean values averaged over 500 days, calculated at 250-day intervals, while data at 1400 MHz are mean values averaged over 2000 days, calculated at 1000-day intervals.

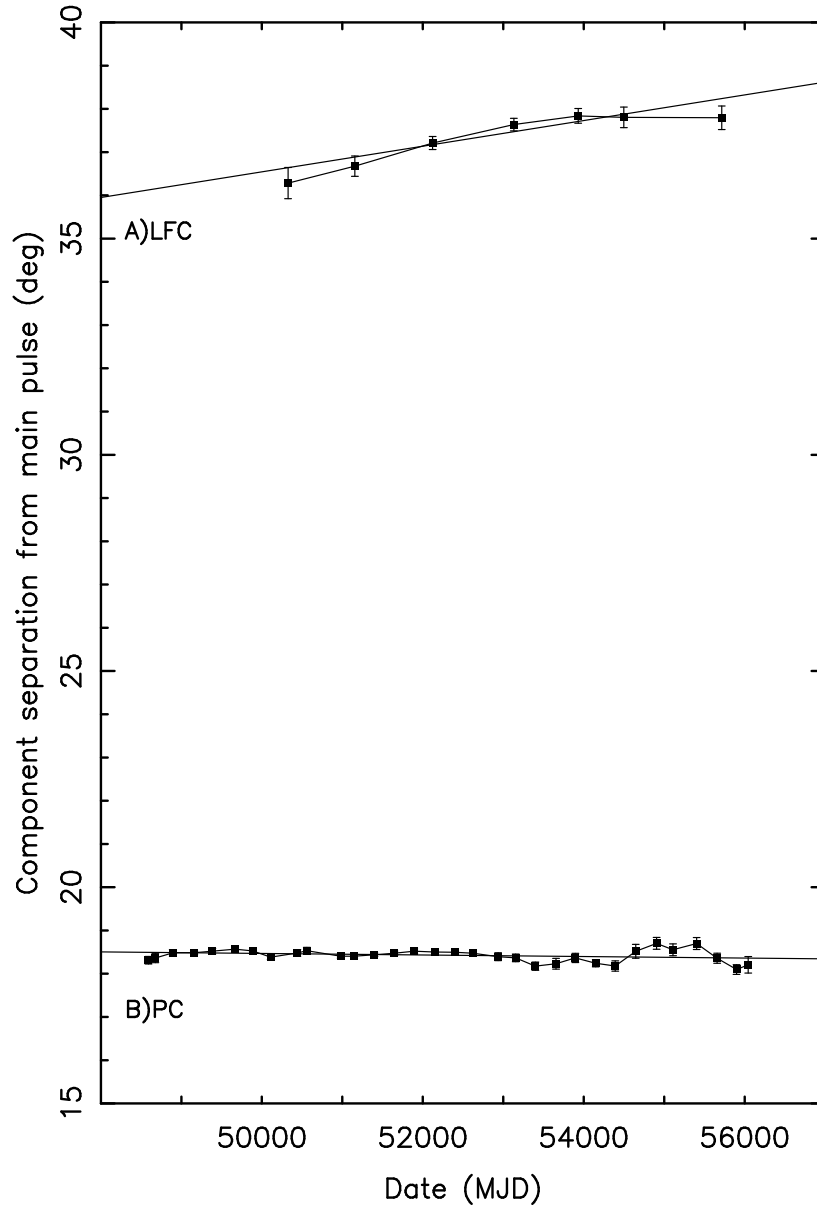


Figure 3: The rotational separation of components of the Crab pulse profile from the MP. A) the LFC at 1400 MHz and B) the PC at 610 MHz. Data at 610 MHz are displayed as mean values averaged over 500 days, calculated at 250-day intervals, while data at 1400 MHz are mean values averaged over 2000 days, calculated at 1000-day intervals.

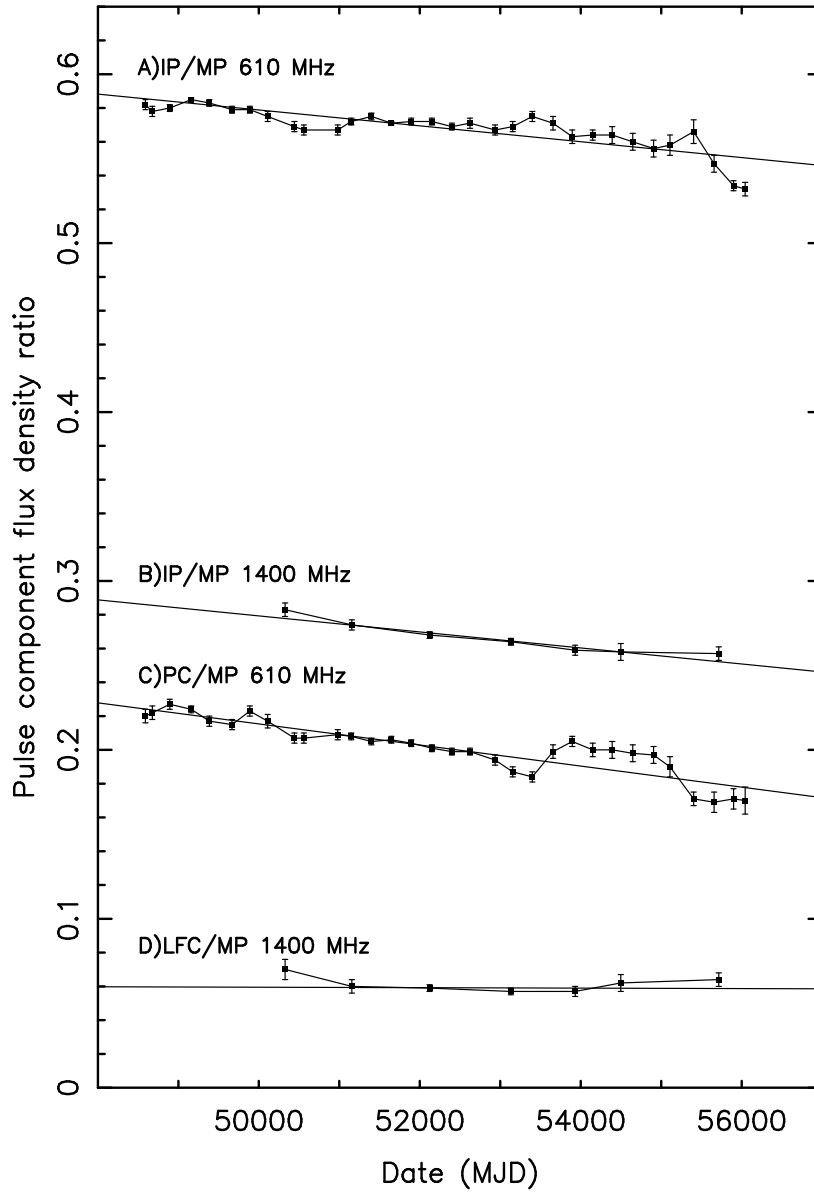


Figure 4: Relative flux densities of Crab pulse profile components. Flux densities are given relative to that of the MP at the same frequency: A) IP at 610 MHz B) IP at 1400 MHz and C) PC at 610 MHz and D) LFC at 1400 MHz. Data at 610 MHz are displayed as mean values averaged over 500 days, calculated at 250-day intervals, while data at 1400 MHz are mean values averaged over 2000 days, calculated at 1000-day intervals.